AGU100 ADVANCING EARTH AND SPACE SCIENCE

Geophysical Research Letters

RESEARCH LETTER

10.1029/2018GL077717

Key Points:
- Proxy-based reconstructions and model-based simulations of global mean surface temperature over the last 800,000 years differ in detail
- During periods of decreasing obliquity and sea level the proxy reconstructions show a temperature-CO_2 divergence missing in simulations
- Elimination of these periods leads to a more linear paleoclimate sensitivity and to equilibrium warming for CO_2 doubling of 2–4 K

Supporting Information:
- Supporting Information S1

Correspondence to:
P. Köhler,
Peter.Koehler@awi.de

Citation:
Köhler, P., Knorr, G., Stap, L. B., Ganopolski, A., de Boer, B., van de Wal, R. S. W., et al. (2018). The effect of obliquity-driven changes on paleoclimate sensitivity during the late Pleistocene. *Geophysical Research Letters*, *45*, 6661–6671. https://doi.org/10.1029/2018GL077717

Received 28 FEB 2018
Accepted 6 JUN 2018
Accepted article online 14 JUN 2018
Published online 13 JUL 2018

©2018. The Authors.
This is an open access article under the terms of the Creative Commons Attribution-NonCommercial-NoDerivs License, which permits use and distribution in any medium, provided the original work is properly cited, the use is non-commercial and no modifications or adaptations are made.

The Effect of Obliquity-Driven Changes on Paleoclimate Sensitivity During the Late Pleistocene

Peter Köhler[1], Gregor Knorr[1], Lennert B. Stap[1], Andrey Ganopolski[2], Bas de Boer[3], Roderik S. W. van de Wal[3], Stephen Barker[4], and Lars H. Rüpke[5]

[1]Alfred-Wegener-Institut Helmholtz-Zentrum für Polar-und Meeresforschung (AWI), Bremerhaven, Germany, [2]Potsdam Institute for Climate Impact Research (PIK), Potsdam, Germany, [3]Institute for Marine and Atmospheric research Utrecht (IMAU), Utrecht University, Utrecht, Netherlands, [4]School of Earth and Ocean Science, Cardiff University, Cardiff, UK, [5]GEOMAR Helmholtz Centre for Ocean Research Kiel, Kiel, Germany

Abstract We reanalyze existing paleodata of global mean surface temperature ΔT_g and radiative forcing ΔR of CO_2 and land ice albedo for the last 800,000 years to show that a state-dependency in paleoclimate sensitivity S, as previously suggested, is only found if ΔT_g is based on reconstructions, and not when ΔT_g is based on model simulations. Furthermore, during times of decreasing obliquity (periods of land ice sheet growth and sea level fall) the multimillennial component of reconstructed ΔT_g diverges from CO_2, while in simulations both variables vary more synchronously, suggesting that the differences during these times are due to relatively low rates of simulated land ice growth and associated cooling. To produce a reconstruction-based extrapolation of S for the future, we exclude intervals with strong ΔT_g-CO_2 divergence and find that S is less state-dependent, or even constant state-independent), yielding a mean equilibrium warming of 2–4 K for a doubling of CO_2.

Plain Language Summary Anthropogenic carbon dioxide (CO_2) emissions will lead to rising global mean temperature through the greenhouse effect. The amplitude of this warming, as estimated with computer simulations for the equilibrium climate response to a doubling of atmospheric CO_2 concentration, is called climate sensitivity. It is necessary to verify these simulation-based quantifications of climate sensitivity with independent alternative approaches. One such approach is the analysis of past (paleo) climates, which has indicated a state-dependent paleoclimate sensitivity. Here we compare different data-based reconstructions and computer-based simulations of paleoclimate sensitivity of the last 800,000 years and find that they disagree. In data-based reconstructions global mean temperature and CO_2 diverge during intervals when land ice growth is particularly pronounced. This temperature-CO_2 divergence is not observed in simulations, probably due to an underestimation of the rate of land ice growth and the associated cooling. However, these periods of pronounced land ice growth are not of relevance for a warming future and can therefore be neglected when estimating climate sensitivity from reconstructions of the past. Consequently, we find that paleoclimate sensitivity derived from reconstructions is less state-dependent than previously thought and agrees with warming estimates of 2–4 ° C as derived from simulated equilibrium climate response for CO_2 doubling.

1. Introduction

Analyses of paleoreconstructions (Köhler et al., 2015; K2015 in the following) and paleoclimate simulations (Friedrich et al., 2016; F2016 in the following), covering the late Pleistocene, have suggested that climate sensitivity might not be a constant parameter of the climate system but a state-dependent variable that increases toward warmer climates. Most other studies on this topic indicate a similar behavior, including a review that covers a wide range of colder and warmer climate states (von der Heydt et al., 2016). However, there have also been studies using general circulation models (GCMs) or Earth system models of intermediate complexity (EMICs) which simulate an increase in climate sensitivity for colder than present-day climate (e.g., Colman & McAvaney, 2009; Kutzbach et al., 2013; Pfister & Stocker, 2017).

Fueled by this ambiguity we wanted to test the robustness of the conclusions in earlier studies (K2015 and F2016). Here we investigate whether this, previously found, state-dependency of climate sensitivity can be reproduced in other setups; we reanalyze the proxy-based reconstructions of global temperature change (ΔT_g) published in the last few years (Snyder, 2016, in addition to K2015 and F2016), investigate transient 800-kyr simulation results obtained with the EMICs, CLIMBER (Ganopolski & Calov, 2011), and LOVECLIM (F2016), and analyze the only available transient GCM simulation across the last glacial/interglacial transition provided by the CCSM3 model (He, 2011; Liu et al., 2009; Figure 1).

A direct comparison of today's anthropogenic warming with paleodata-based reconstructions is not possible, due to the lack of a direct analog in the magnitude of the rate of changes. However, we can evaluate the general climate system response to radiative forcing anomalies. For such efforts, the specific equilibrium climate sensitivity (ECS) $S_{[X]}$ (or paleoclimate sensitivity) has been defined as the ratio of the global and annual mean surface temperature change (ΔT_g) over the change in radiative forcing ($\Delta R_{[X]}$) caused by the process(es) X (PALAEOSENS-Project Members, 2012)

$$S_{[X]} = \frac{\Delta T_g}{\Delta R_{[X]}} \tag{1}$$

Here we calculate radiative forcing for processes including the greenhouse gas (GHG) effect (CO_2, CH_4, and N_2O) but also other processes, such as the (planetary) albedo effects from land ice (LI), vegetation (VG), and aerosols (AE). The time dependency of the climate to those forcing or feedback processes is not of particular interest in the following but has been addressed elsewhere (e.g., Rohling et al., 2018; Zeebe, 2013). This concept of calculating $S_{[X]}$ was introduced in PALAEOSENS-Project Members (2012) to clarify which forcing is explicitly included when estimating climate sensitivity from paleodata, not to test causation. Furthermore, this approach assumes that different forcing processes have a similar impact on ΔT_g, which is a simplification (e.g., Stap et al., 2018; Yoshimori et al., 2011), that is difficult to overcome in analyses of mainly proxy-based reconstructions. Within the context of Earth system model analysis this ratio $\Delta T_g/\Delta R_{[X]}$ is also called the *climate sensitivity parameter* (e.g., Yoshimori et al., 2011).

The emergence of state-dependency in $S_{[X]}$ implies that the best fit to a scatter plot of ΔT_g versus $\Delta R_{[X]}$ is not linear, but some nonlinear function, for example, a higher-order polynomial (Figure 2a). While the detection of such a nonlinearity is rather straightforward, the quantification of $S_{[X]}$ is more complicated, as described in detail by Köhler, Stap, et al. (2017).

In F2016 two independent estimates of ΔT_g were generated: a purely proxy-based reconstruction based on SST data from 63 records and a simulation with the LOVECLIM model. The estimates of ΔT_g were then averaged and confirmed the state-dependency in $S_{[X]}$ for the last ~800 kyr as deduced by K2015. Since this state-dependency in $S_{[X]}$ suggests that during warm interglacials a relatively small change in ΔR leads to a relatively large change in ΔT_g (Figure 2a), it is crucial to know how robust this conclusion is. Recently, a new proxy-based reconstruction of global mean temperature changes constructed from 61 records of SST anomalies has been published (Snyder, 2016). These two proxy-based reconstructions of ΔT_g (F2016; Snyder, 2016) are not fully independent with respect to the underlying data but differ in details and in the upscaling methodologies.

Finally, we discuss how our findings for paleoclimate sensitivity can be extrapolated to the future and compare a rough approximation of equilibrium global warming caused by 2×CO_2 with other approaches.

2. Methods

In K2015 deconvolution of the LR04 benthic $\delta^{18}O$ stack (Lisiecki & Raymo, 2005) was used to provide mutually consistent contributions from sea level (or land ice volume) and deep ocean temperature (ΔT_O) using 3-D ice sheet models of de Boer et al. (2014). Temperature change over land in the high-latitude Northern Hemisphere (about 40–85°N, ΔT_{NH}) where most glacial/interglacial changes in land ice occurred during the late Pleistocene is linearly related to ΔT_O on a multimillennial time scale. However, ΔT_{NH} also contains changes due to elevation changes (lapse rate) and considers seasonality. ΔT_g and ΔT_{NH} are then related to each other via a nonconstant polar amplification factor (f_{pa}) that has been determined from PMIP3 output. Sensitivity analyses (de Boer et al., 2014; K2015) have shown that ΔT_g has a relative uncertainty of ~10% over the last 800 kyr. This setup is a model-based interpretation of proxy data. It is a mixture between a purely proxy-based reconstruction and model-based simulations. However, while full climate models are driven by temporal changes in various boundary conditions (e.g., insolation and GHG) and then calculate all other variables internally, here only the ice sheet dynamics are simulated. Therefore, we consider our approach to be more similar to those of

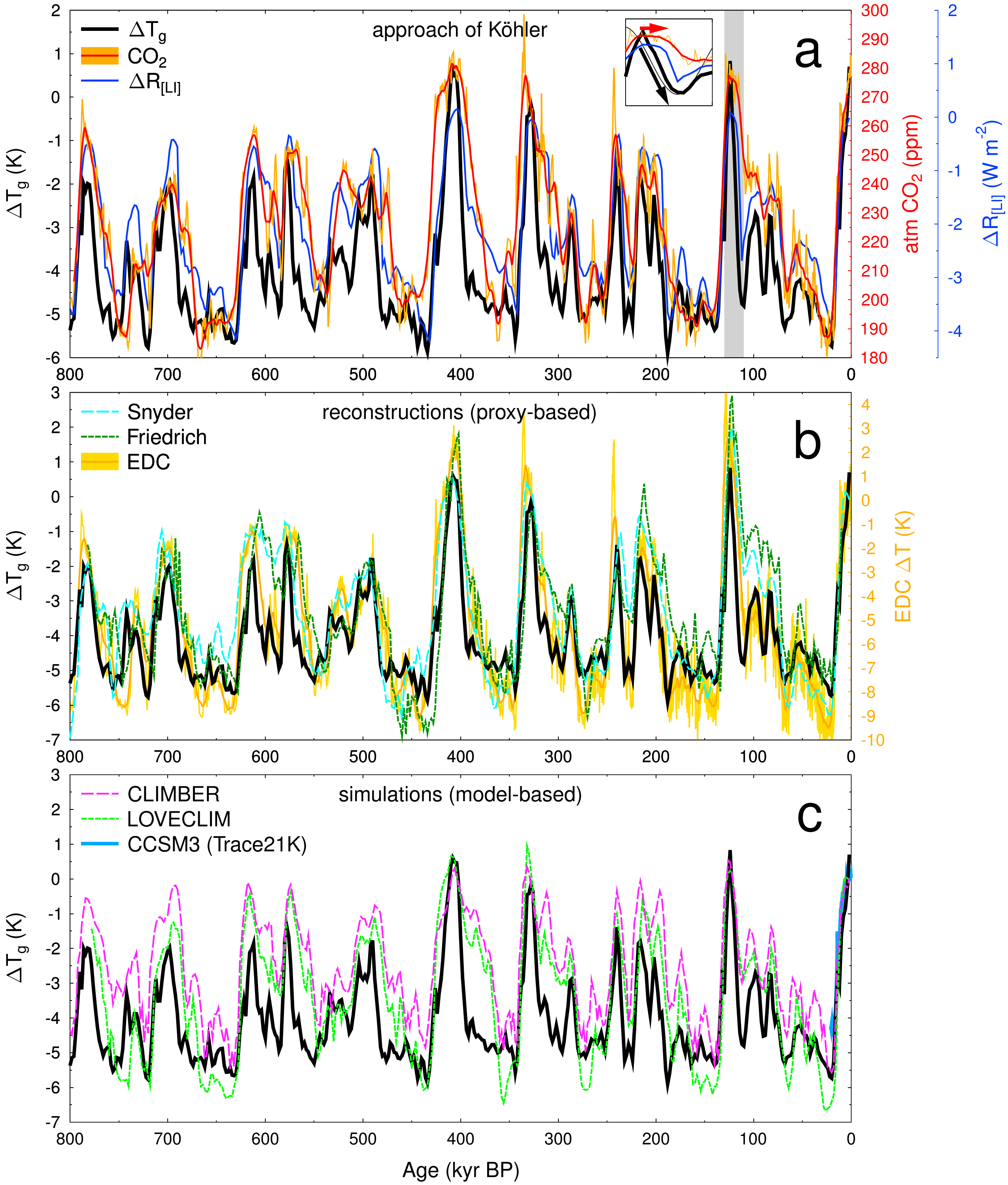

Figure 1. Paleodata of the last 800 kyr. (a) Data used in the approach of Köhler (K2015) with global mean temperature change ΔT_g, land ice-based radiative forcing change $\Delta R_{[LI]}$ and atmospheric CO_2 (Bereiter et al., 2015). Inset shows an enlarged view on the divergence of ΔT_g and CO_2 at the end of the Eemian (130–110 kyr BP, gray band), including as thin black line changes in obliquity (Laskar et al., 2004). Comparing different temperature time series with K2015-ΔT_g (black bold line); (b) proxy-based reconstructions of ΔT_g (Synder, Friedrich (F2016)) and EPICA Dome C (EDC) ΔT; (c) model-based simulations (CLIMBER and LOVECLIM) including CCSM3 for the last 21 kyr. Ice core data (EDC ΔT, CO_2) are plotted on the most recent age model AICC2012 (Bazin et al., 2013; Veres et al., 2013) and shown as original high-resolution data (thin) and 8-kyr running means (bold).

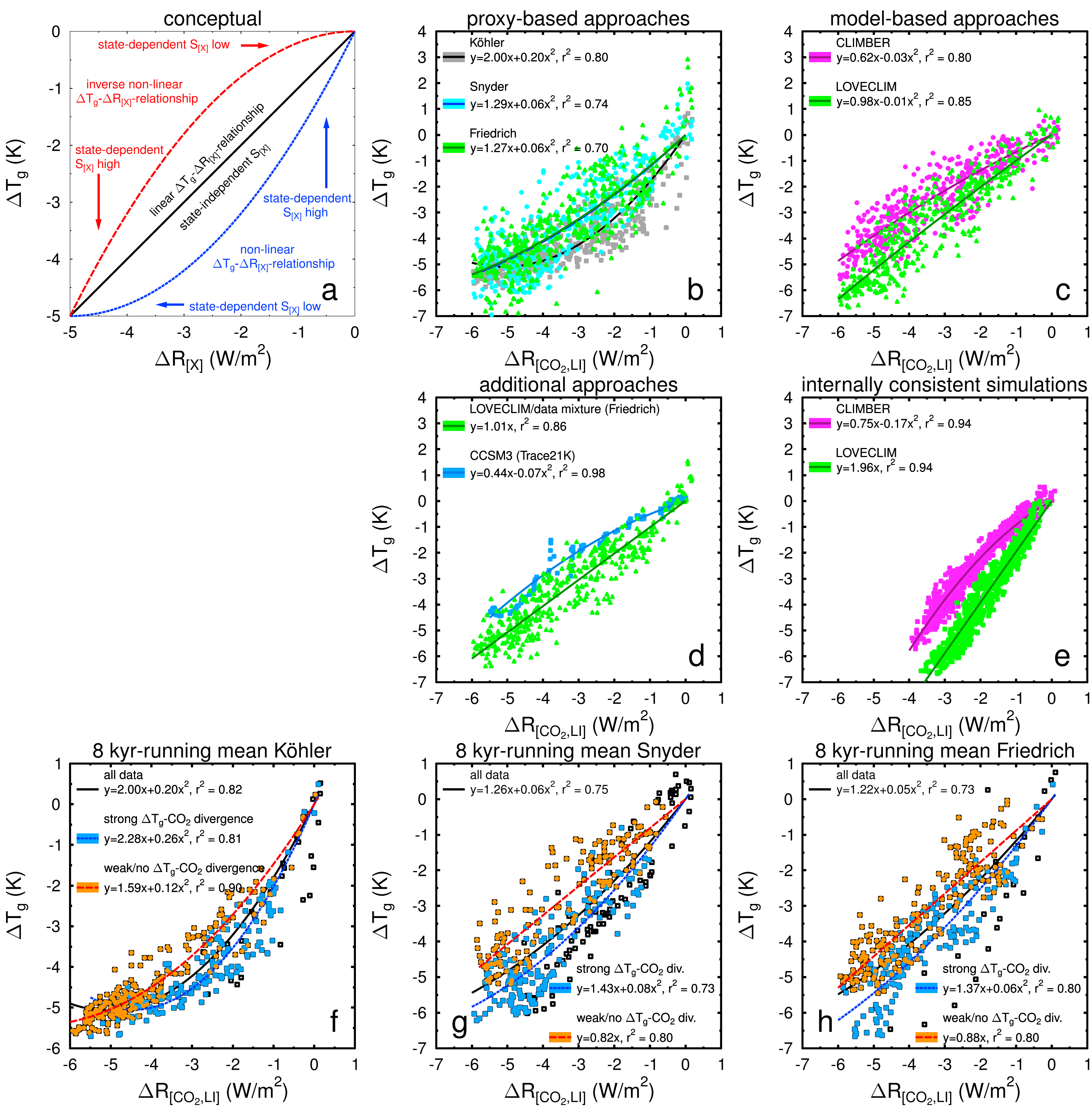

Figure 2. Scatter plots of temperature change ΔT_g over radiative forcing change $\Delta R_{[X]}$. (a) Conceptual understanding of different relationships between ΔT_g and $\Delta R_{[X]}$ and the resulting state-(in)dependency of $S_{[X]}$. (b) Data-based reconstructions of ΔT_g (Köhler, Snyder, and Friedrich); (c) model simulation results of ΔT_g (CLIMBER and LOVECLIM); (d) alternative approaches (Friedrich's model/data mixture for ΔT_g, 21 kyr transient simulations with CCSM); (e) internally consist model setups of CLIMBER and LOVECLIM; (f–h) multimillennial component (8-kyr running mean) of the proxy-based approaches (f: Köhler; g: Snyder; h: Friedrich) split in time windows with strong or weak divergence of ΔT_g and CO_2. Data are split by the zero line in the standardized ratio $\Delta T_g/\Delta R_{[CO_2]}$ shown in Figure 3b. White squares are data points which are filtered out in the standardizing of the data, and therefore neither considered in strong or weak divergence part, but which contribute to the fit through all data. In most plots the same $\Delta R_{[CO_2,LI]}$ from K2015 is plotted, while in (d) CCSM3 is based on $\Delta R_{[LI]}$ from ICE-5G; in (e) we show $\Delta R_{[CO_2,LI]}$ as used in CLIMBER and LOVECLIM.

10.1029/2018GL077717

the proxy-based reconstructions than of the model-based simulations. From the three alternative time series, based on different assumptions for the polar amplification factor f_{pa} in K2015, we use the standard case (ΔT_{g1}), in which f_{pa} is linearly related to ΔT_{NH}. However, our conclusions are not dependent on this choice of f_{pa} and ΔT_g (see the application of the alternative temperature time series in Figure S1 in the supporting information). The fact that three alternative formulations of ΔT_g can be connected to the same $\Delta R_{[LI]}$ shows that there are some degrees of freedom in the connection of both variables.

In K2015 the radiative forcing of CO_2 ($\Delta R_{[CO_2]} = 5.35 \cdot \ln(CO_2/(278\,\mathrm{ppm}))\,\mathrm{W/m^2}$, Myhre et al. (1998)) and land ice albedo was considered explicitly—leading to $\Delta R_{[CO_2,LI]}$ and to the state-dependency in $S_{[CO_2,LI]}$. It should be noted that when following the revised formulation of Etminan et al. (2016), $\Delta R_{[CO_2]}$ differs by less than 0.01 W/m^2 (Köhler, Nehrbass-Ahles, et al., 2017). Furthermore, we assume that radiative forcing is state-independent, which might be a simplification (e.g., Forster et al., 2016). We will analyze similar variables based on alternative ΔT_g from proxies (F2016; Snyder, 2016) and simulations (LOVECLIM (F2016), CLIMBER (Ganopolski & Calov, 2011), CCSM3 (He, 2011; Liu et al., 2009)). We will first analyze these different ΔT_g in relation to the same $\Delta R_{[CO_2,LI]}$ as derived in K2015, but for in-depth investigations of simulations we only use the internally applied radiative forcing. The use of these alternative ΔT_g for identical $\Delta R_{[CO_2,LI]}$ has the potential to introduce a bias because temperature and land ice distribution are firmly linked through deconvolution of the LR04 benthic δ^{18}O stack. This potential bias is not investigated any further here, although alternative land ice distribution (e.g., ICE-5G of Peltier, 2004) agrees well with our results (K2015). Alternative approaches to estimate $\Delta R_{[LI]}$ from sea level changes have shortcomings, since they omit the latitudinal effect of land ice distribution on radiative forcing (see K2015 for further details). Chronological misfits between the different records, which might also be introduced in that way, should not be of importance here, as our final interpretations are based on 8-kyr running means. Details of both alternative $\Delta R_{[LI]}$ estimates and chronological issues have been discussed previously (K2015; Köhler, Stap, et al., 2017). For the CLIMBER simulations additional processes (CH_4, N_2O, vegetation, and aerosols) in the radiative forcing term $\Delta R_{[X]}$ are also considered.

Time series are standardized before analysis. Due to very high variability in calculated ratios (Figures 3b and 3c, and S1b and S1c) data far away from the mean ($|\Delta T_g/\Delta R_{[CO_2,LI]}| > 0.25\sigma$; $|\Delta R_{[LI]}/\Delta R_{[CO_2]}| > 1\sigma$) are considered as outliers and removed. The chosen cutoff thresholds mainly influence the peak height in the standardized time series, but not the dynamics contained in the time series. Due to the rather linear behavior of the simulations, no outliers in $\Delta T_g/\Delta R_{[CO_2,LI]}$ have been removed from the LOVECLIM and CLIMBER results. Finally, the outlier-free time series are standardized a second time to enable comparison between the different approaches. This outlier selection during standardization is illustrated for K2015 in Figure S2.

The land ice dynamics simulated in CLIMBER (which are also used in LOVECLIM via off-line coupling) are restricted to Northern Hemisphere ice sheets, Antarctic land ice is kept fixed at present-day configuration, while in K2015 the dynamics of ice sheets and ice shelves in both hemispheres have been investigated. The CCSM3 simulations (He, 2011; Liu et al., 2009) were driven by the ICE-5G land ice distribution, which was compared to de Boer et al. (2014) in K2015. This ICE-5G-based $\Delta R_{[LI]}$ is also used here when investigating CCSM3 results.

We use the internal fitting routines of the software package GLE, the Graphics Layout Engine (http://www.gle-graphics.org) and use *F* tests to determine whether a second-order polynomial fits the scattered ΔT_g-ΔR data better than a linear approach (Table S1). For all fits the precondition of meeting the origin is applied (no temperature change for no forcing change), leading to the following two regression equations to be tested: either $y = b \cdot x$ (linear) or $y = b \cdot x + c \cdot x^2$ (nonlinear).

In cases where uncertainties in both ΔT_g and $\Delta R_{[X]}$ are available, more elaborate statistics might be applied (e.g., Monte Carlo approaches have been used in K2015). Uncertainties in ΔT_g are only available for K2015 and Snyder. In Figure S3, we show that nonlinear fits are very similar when considering or ignoring uncertainties in these two data sets. We take this as support for the more simplistic approach in our main analysis: all data sets are treated identically and fits are calculated without considering uncertainties in the scattered data.

3. Results and Discussions

3.1. Proxy-Based Reconstructions Versus Model-Based Simulations

The main difference between proxy-based reconstructions and model-based simulations to estimate global temperature changes is that the proxy-based reconstructions capture the impacts of all Earth system processes active in the considered time window, while in the model-based approaches only those processes

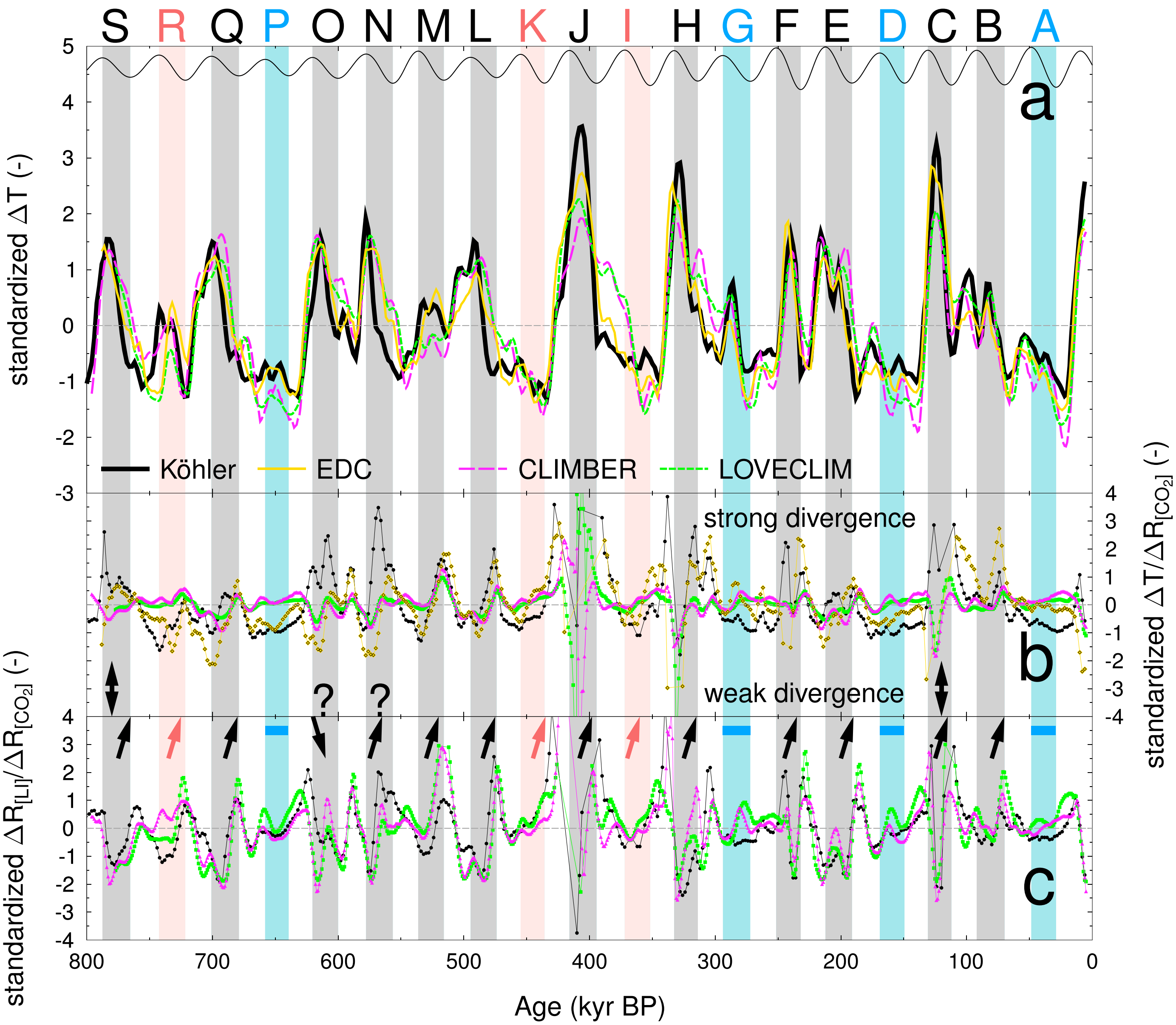

Figure 3. Multimillennial (all data as 8-kyr running mean) ΔT-CO_2 divergence and relative contributions of radiative forcing of land ice albedo and CO_2 for ΔT in different setups. (a) ΔT (local ΔT for EDC and ΔT_g elsewhere); (b) the divergence of ΔT and CO_2 described by $\Delta T/\Delta R_{[CO_2]}$; (c) $\Delta R_{[LI]}/\Delta R_{[CO_2]}$: Relative land ice (sea level) contribution with respect to CO_2. The data sets Köhler and EDC differ only by their ΔT. From the model simulations (CLIMBER and LOVECLIM) we analyzed the internally used radiative forcing. All data sets have been standardized and outliers in the ratios have been filtered out. Obliquity (Laskar et al., 2004) is sketched on top of subpanel a (thin black line), with shadings and labels (A–S) indicating times of decreasing obliquity. Color code is given by the details of the Köhler data set: Gray = strong ΔT_g-CO_2 divergence including large variations in relative sea level contribution; light red = no or weak ΔT_g-CO_2 divergence and large variations in relative sea level contribution; light blue = no or weak ΔT_g-CO_2 divergence and stable relative sea level contribution. Vertical two-headed arrows in the ΔT_g-CO_2 divergence panel indicate the antiphase dynamics partially seen between Köhler and the CLIMBER/LOVECLIM data sets. Question marks in (b) highlight two phases (MIS 15a and MIS15e) during which Köhler and EDC largely disagree.

implemented in the model can leave their imprint in the simulation results. Simulated time series of ΔT_g, therefore, have to be questioned critically for any serious omissions. In other words, any persisting difference between proxy-based reconstructions and simulated ΔT_g might be caused by those processes not included in the models. Alternatively, proxy-based reconstructions might be systematically biased, although this seems unlikely if independent reconstructions come to similar conclusions.

Here we compare results of others to the approach of K2015 (Figure 1a) in order to understand when the proposed state-dependency in $S_{[CO_2,LI]}$ is sustained or when it needs to be rejected. If we replace ΔT_g with an alternative time series (F2016, Snyder, CLIMBER, LOVECLIM, CCSM3, Figures 1b and 1c), we find a similar state-dependency in $S_{[CO_2,LI]}$ — with higher values for warmer conditions — when the applied ΔT_g time series is based on proxy-based reconstructions (Figure 2b). This holds for the temperature data set of Snyder, as well as for proxy-based ΔT_g derived in F2016 (Figure 2b). The nonlinearity in the ΔT_g-$\Delta R_{[CO_2,LI]}$ scatter plots is less pronounced in these alternative calculations, when compared to K2015.

If temperature anomalies are taken from CLIMBER simulations, a nonlinear relationship between ΔT_g and $\Delta R_{[CO_2,LI]}$ is generated that is inverse to that found by K2015 (Figure 2c), suggesting a smaller paleoclimate sensitivity for warmer climates. Similarly, if we base this analysis on the ΔT_g simulated in LOVECLIM, we find an inverse nonlinear relationship — opposite to the proxy-based results (Figure 2c). Since the ΔT_g-$\Delta R_{[CO_2,LI]}$ relationship of the proxy-based reconstructions of F2016 and the transient LOVECLIM simulations show the opposite slope, it is natural that an averaged ΔT_g based on both (as used in F2016) contains a rather linear relationship (Figure 2d). Finally, we analyzed the only available transient GCM-simulation, the Trace21K scenario of the CCSM3 model for the last 21 kyr. Using their ΔT_g, we again find the same results as from the EMIC runs (Figure 2d) — a state-dependent paleoclimate sensitivity with steeper slopes in the ΔT_g-$\Delta R_{[CO_2,LI]}$ data during colder climates, pointing to a higher $S_{[CO_2,LI]}$, which is inverse to the results from the proxy-based approaches.

If we analyze internally consistent EMIC simulation results using the radiative forcing of CO_2 and land ice applied in the model runs together with the simulated ΔT_g (instead of $\Delta R_{[CO_2,LI]}$ based on K2015), we find a linear relationship between ΔT_g and $\Delta R_{[CO_2,LI]}$ for LOVECLIM (Figure 2e). In CLIMBER we find a similar nonlinear relationship between ΔT_g and $\Delta R_{[CO_2,LI]}$ — with steeper slope during cold climate — as in the approaches in which the CLIMBER-simulated ΔT_g was analyzed together with $\Delta R_{[CO_2,LI]}$ of K2015 (Figure 2e). Further details on the differences in $\Delta R_{[LI]}$ for the different approaches can be found in Figure S4.

3.2. Obliquity-Driven Changes and the ΔT_g-CO_2 Relationship

How can we understand this strong state-dependency of S found in proxy-based approaches and the difference to the model-based approaches? It has recently been deduced, from ice core data covering the last 800 kyr, that the multimillennial trend of atmospheric CO_2 concentration and Antarctic temperature diverge when obliquity decreases (Hasenclever et al., 2017). One way of perceiving this divergence is that the reduced incoming insolation at high latitudes causes land ice sheet growth and cooling, while there is a coexisting process that keeps CO_2 at a relatively constant level. Solid Earth modeling experiments have indicated that falling sea level might lead to enhanced magma and CO_2 production at mid-ocean ridges (e.g., Lund & Asimow, 2011). Hasenclever et al. (2017) suggested that the combination of marine volcanism at mid-ocean ridges and at hot spot island volcanoes might react to decreasing sea level and be a potential cause for this ΔT_g-CO_2 divergence. Alternatively, the divergence implies that processes other than CO_2 radiative forcing or land ice albedo (potentially radiative forcing from non-CO_2 GHGs, or albedo change caused by aerosols, or vegetation) dominate during these phases — leading to a cooling with little reduction in CO_2. The evidence so far (e.g., Köhler et al., 2010) does not indicate that the latter was the case, although potential impacts of different forcing efficacy (e.g., Stap et al., 2018; Yoshimori et al., 2011) have so far not been investigated. One study analyzed the contribution of the terrestrial carbon cycle to the divergence of CO_2 and ΔT_g at the end of the present (Holocene) and the previous (Eemian or MIS 5e) interglacial (Brovkin et al., 2016). Processes which seemed to explain the reconstructed divergence in the Holocene failed to explain similar dynamics during MIS 5e, pointing to model deficiencies in the representation of the land carbon cycle, or suggesting that other processes are at work. All modeling results used in here (CLIMBER, LOVECLIM, and CCSM3) were obtained in simulations with prescribed observed CO_2 concentrations and thus include all effects of the Earth system feedbacks on CO_2. However, simulation results do not contain the characteristic long-term ΔT_g-CO_2 divergence found in the proxy-based reconstructions (Snyder, F2016), or in the deconvolution of LR04-δ^{18}O into land ice dynamics (K2015). This suggests that a relatively low rate of simulated land ice growth and associated cooling during times of decreasing obliquity, and not a feedback on CO_2, might be responsible for the difference between model- and proxy-based approaches.

When ΔT_g is derived mainly from proxy-based reconstructions (K2015, F2016, and Snyder), our results show a strong ΔT_g-CO_2 divergence at times of obliquity decrease. An example of this is the dynamics at the end of the Eemian (see zoom-in in the inset in Figure 1a). For comparison of the different approaches, all time series in the following are analyzed in their standardized versions (Figures 3 and S1). They confirm the earlier finding of a temperature-CO_2 divergence at times of obliquity decrease by Hasenclever et al. (2017), in which not global temperature change, but Antarctic temperature change derived from the EPICA Dome C (EDC) ice core (Jouzel et al., 2007) has been considered. The temporal evolution of this divergence between ΔT_g and CO_2 can be observed by analyzing the multimillennial dynamics of the ratio $\Delta T_g/\Delta R_{[CO_2]}$, which by coincidence is also defined as $S_{[CO_2]}$ (Figure 3b). The interpretation of $S_{[CO_2]}$ as a proxy for the multimillennial ΔT_g-CO_2-divergence represents a major improvement in the understanding of $S_{[CO_2]}$, since previously no meaningful patterns have been detected in its temporal variability (PALAEOSENS-Project Members, 2012). We find that a strong ΔT_g-CO_2 divergence exists in 12 out of 19 phases with decreasing obliquity (gray bands in Figure 3) in the data from K2015. Furthermore, the ratio of land ice and CO_2 radiative forcing ($\Delta R_{[LI]}/\Delta R_{[CO_2]}$) underwent large changes during these intervals (Figure 3c), suggesting that land ice (sea level) related changes might indeed be connected to the times of these diverging trends.

The seven phases with decreasing obliquity, but without strong ΔT_g-CO_2 divergence in K2015, can furthermore be divided into periods with a stable ratio of $\Delta R_{[LI]}/\Delta R_{[CO_2]}$ (light blue bands marked A, D, G, and P) and those with strong variability in $\Delta R_{[LI]}/\Delta R_{[CO_2]}$ (light red bands I, K, and R). In the former periods (blue colored) the stable ratio of land ice and CO_2 radiative forcing suggests in-phase variations of both processes, which might indicate that any potential sea level-related CO_2 outgassing from marine volcanism or other processes could be compensated by the land ice sheet albedo feedback. In the latter periods (red colored) the ratio $\Delta T_g/\Delta R_{[CO_2]}$ is always increasing toward the end of the obliquity-half cycle, suggesting that some sea level-related process affecting CO_2 might have initiated but not yet developed its full potential. This leads, for example, to the unusual strong ΔT_g-CO_2 divergence after the end of period K at 436 kyr BP which persisted for almost a complete obliquity cycle around MIS 11. Five of these seven phases with decreasing obliquity but without a strong ΔT_g-CO_2 divergence (A, D, I, K, and P, but not G and R) are also characterized by very modest cooling, indicating that the net climate changes during these phases are small when compared to other phases with decreasing obliquity. These phases should, therefore, be interpreted with care since the dominant climate variations occur during other times.

Much smaller variations in the ΔT_g-CO_2 divergence are found when analyzing model-based simulations of CLIMBER and LOVECLIM than in K2015 (Figure 3b). Furthermore, the model-based ΔT_g-CO_2 divergence observed during times of decreasing obliquity is partially in antiphase to the proxy-based results (phases C and S), suggesting highly synchronous variations in CO_2 and simulated ΔT_g while a strong divergence to CO_2 persists in the reconstructed ΔT_g (Figure 3b). The two lukewarm interglacials MIS 15a, and 15e (phases N, O, 570 and 610 kyr BP, respectively, Past Interglacials Working Group of PAGES, 2016) seem to be special in this respect, since the ΔT_g-CO_2 divergence from K2015 is in antiphase to those based on the simulation output and also to that based on EDC ΔT. Interestingly, the temperature-CO_2 divergence during the MIS 5/4 transition, around 75 kyr BP (phase B) which motivated the study of Hasenclever et al. (2017), is one of the largest in EDC but rather weak in K2015. Our calculated ΔT_g-CO_2 divergence, based on ΔT_g of Snyder or F2016, contains qualitatively similar dynamics related to obliquity as that based on EDC ΔT or K2015 but differs from the model-based simulations (Figure S1). This qualitative agreement of the divergence in proxy-based ΔT_g (K2015, F2016, Snyder, and EDC) provides confidence in the global temperature record obtained in K2015. Furthermore, tests have shown that if new insights into polar amplification (Stap et al., 2018) are used for an improvement of the model setup used in K2015, only small changes in ΔT_g are generated, but the general difference to the model-based simulations persists. Based on these findings, the analysis of Hasenclever et al. (2017) needs to be expanded: decreasing obliquity seems to be a necessary but not a sufficient condition for the ΔT_g-CO_2 divergence. Another process related to sea level change, or in detail to $\Delta R_{[LI]}/\Delta R_{[CO_2]}$, needs to be active at the same time to explain the data.

The importance of this ΔT_g-CO_2 divergence and its connection to obliquity, for the state-dependency of our paleoclimate sensitivity estimate, becomes apparent when we split the data into times with increasing or decreasing obliquity. In the latter case the nonlinearity (parameter *c* in the second-order fit) between ΔT_g and ΔR is significantly different in the data set of K2015 and Snyder (Figures S5a and S5c), while in the CLIMBER output hardly any difference can be detected (Figure S5b). For F2016 (Figure S5d), which shows a nonlinear relationship when all data are analyzed, the relationship is only linear in both data subsets when differentiated by their phase of obliquity. When data are split based on the ratio $\Delta T_g/\Delta R_{[CO_2]}$ in subsets with strong or weak ΔT_g-CO_2 divergence, we find an even larger difference in the nonlinearity than when data are split by obliquity in K2015 (Figure 2f), implying a more linear relationship for data with strong ΔT_g-CO_2 divergence than for data with decreasing obliquity. When using ΔT_g from the proxy-based reconstructions of Snyder and F2016, we find a nonlinear relationship in the ΔT_g-$\Delta R_{[CO_2,LI]}$ scatter plot during strong ΔT_g-CO_2 divergence, while for times with more synchronous changes in ΔT_g and CO_2 (weak divergence) a linear relationship between ΔT_g and $\Delta R_{[CO_2,LI]}$ emerges (Figures 2g and 2h).

3.3. Using Paleoclimate Sensitivity to Estimate $\Delta T_{2\times CO_2}$

The ΔT_g-CO_2 divergence appears mainly during, or in connection with, periods of decreasing obliquity related to land ice growth or sea level fall. These times cover ~50% of past climates. We conclude that for a generic climate system understanding the implementation of the processes responsible for this ΔT_g-CO_2 divergence, potentially being the solid Earth-climate feedbacks related to a sea level-induced change in marine volcanism (e.g., Hasenclever et al., 2017; Lund & Asimow, 2011), is essential.

Intervals of strong ΔT_g-CO_2 divergence should not be considered for the interpretation of paleodata in the context of future warming, for example, by calculating the paleoclimate sensitivity S, because in the future we expect sea level to rise. Otherwise the climate system response of a glaciation is erroneously implicated with anthropogenic warming. Here one might rely only on the subset of ΔT_g-ΔR data that coincide with times of weak (or no) ΔT_g-CO_2 divergence. For K2015, this restriction would lead to a different quantification of paleoclimate sensitivity following the framework of Köhler, Stap, et al. (2017; Figure 2f). In detail, $S_{[CO_2,LI]}$ can be derived from the fit to the scattered ΔT_g-$\Delta R_{[CO_2,LI]}$ data after $S_{[CO_2,LI]} = b + c \cdot \Delta R_{[CO_2,LI]}$. The paleodata of the last 800 kyr cover mainly intervals with $\Delta R_{[CO_2,LI]} \leq 0$ W/m^2, and due to the state-dependent character of $S_{[CO_2,LI]}$ we refrain from an extrapolation of our derived fitting function to a range not covered by the data, for example, to $\Delta R_{[CO_2,LI]} > 0$ W/m^2. Nevertheless, climates comparable to late Pleistocene interglacials can be approximated by $\Delta R_{[CO_2,LI]} \approx 0$ W/m^2. $S_{[CO_2,LI]}$ for those interglacials would be ~20% smaller when excluding intervals of ΔT_g-CO_2 divergence in comparison to calculations based on all available data, $S_{[CO_2,LI]} = 1.6$ K/(W/m^2) instead of 2.0 K/(W/m^2). If based on ΔT_g of Snyder (Figure 2g) or F2016 (Figure 2h) these subsets of data with weak (or no) ΔT_g-CO_2 divergence are defined by a linear relationship between ΔT_g and $\Delta R_{[CO_2,LI]}$ and a constant $S_{[CO_2,LI]}$ of 0.82 and 0.88 K/(W/m^2), respectively. To estimate equilibrium warming caused by 2×CO_2 ($\Delta T_{2\times CO_2}$, the classical Charney ECS (Charney et al., 1979; Knutti et al., 2017) from our $S_{[CO_2,LI]}$), we need to correct for missing slow processes (radiative forcing of CH_4 and N_2O; albedo changes caused by vegetation and aerosols). In a previous study (PALAEOSENS-Project Members, 2012) the ratio between $S_{[GHG,LI,VG,AE]}/S_{[CO_2,LI]}$ for the last 800 kyr has been determined as $0.64 \pm 0.07\,(1\sigma)$. Note that this correction for the slow processes ignores any state-dependency that might be associated with them. Together with the average radiative forcing for a doubling of CO_2 of 3.71 W/m^2 ($\pm 10\%(1\sigma)$) (Myhre et al., 1998) our $S_{[CO_2,LI]}$ for late Pleistocene interglacials translates into a $\Delta T_{2\times CO_2}$ or ECS of 1.9 ± 0.3 K (Snyder), 2.1 ± 0.3 K (F2016), and 3.8 ± 0.6 K (K2015). Alternative calculations, based on the data split by obliquity (Figure S5), would lead to slightly larger numbers of ECS (2.3 ± 0.3 K (Snyder), 2.3 ± 0.3 K (F2016), and 4.4 ± 0.7 K (K2015)); however, we consider these to be less reliable following our analysis in the previous subsection. This compares well with other approaches (Knutti et al., 2017), including the narrow *likely* (66% confidence interval) range of 2.2–3.4 K recently obtained from an emerging constraint from global temperature variability and CMIP5 (Cox et al., 2018), and the 95% confidence range of 2.0–4.3 K from a large model ensemble, which has been constrained by observational and geological evidences (Goodwin et al., 2018).

4. Conclusions

In conclusion, we find an inconsistency in the state-dependency of paleoclimate sensitivity calculated from model simulations and proxy-reconstructions, when explicitly considering radiative forcing of CO_2 change and land ice albedo change, or $S_{[CO_2,LI]}$. This may be related to the fact that fast climate feedbacks in EMICs are too linear. Furthermore, EMICs may underestimate the strength of some slow climate feedbacks. As it has been shown that solid Earth-climate feedbacks can play an important role for CO_2 dynamics during glacial cycles (e.g., Hasenclever et al., 2017; Huybers & Langmuir, 2009; Lund & Asimow, 2011), these feedbacks should be incorporated in models used to simulate CO_2 concentration (e.g., Ganopolski & Brovkin, 2017). Furthermore, one also needs to fully understand why current model simulations contain none of the temperature-CO_2 divergence observed during intervals of decreasing obliquity within proxy-based reconstructions. Our study suggests that one possible reason for this discrepancy is that the CLIMBER model underestimates the rate of land ice growth during periods of decreasing obliquity and consequently simulates less cooling induced by land ice. It should be emphasized that the magnitude of the expected CO_2 changes connected with these solid Earth feedbacks are small when compared with anthropogenic CO_2 changes. Therefore, these missing model feedbacks in CLIMBER do not affect its ability to simulate future temperature increase caused by a rise in CO_2. Our results have important consequences for future efforts to quantify paleoclimate sensitivity from proxy-based analyses. We suggest that studies should focus on intervals without decreasing obliquity or sea level, since the detected divergence of global temperature and CO_2 during these intervals could otherwise overprint the system response.

Acknowledgments
This is work institutional-funded at AWI via the research program PACES-II of the Helmholtz Association. It contributes to PALMOD, the German Paleomodeling Research Project funded by BMBF. Gregor Knorr acknowledges funding by Helmholtz Climate Initiative REKLIM (Regional Climate Change), a joint research project of the Helmholtz Association of German research centers (HGF). B. de Boer is funded by NWO Earth and Life Sciences (ALW), project 863.15.019. This work contributes to the Netherlands Earth System Science Centre (NESSC). We thank Tobias Friedrich for providing data and Emma Smith for language editing. No new data have been generated for this work. All analyzed data sets have been taken from the cited literature.

References

Bazin, L., Landais, A., Lemieux-Dudon, B., Toyé Mahamadou Kele, H., Veres, D., Parrenin, F., et al. (2013). An optimized multi-proxy, multi-site Antarctic ice and gas orbital chronology (AICC2012): 120–800 ka. *Climate of the Past*, *9*(4), 1715–1731. https://doi.org/10.5194/cp-9-1715-2013

Bereiter, B., Eggleston, S., Schmitt, J., Nehrbass-Ahles, C., Stocker, T. F., Fischer, H., et al. (2015). Revision of the EPICA Dome C CO_2 record from 800 to 600 kyr before present. *Geophysical Research Letters*, *42*, 542–549. https://doi.org/10.1002/2014GL061957

Brovkin, V., Brücher, T., Kleinen, T., Zaehle, S., Joos, F., Roth, R., et al. (2016). Comparative carbon cycle dynamics of the present and last interglacial. *Quaternary Science Reviews*, *137*, 15–32. https://doi.org/10.1016/j.quascirev.2016.01.028

Charney, J. G., Arakawa, A., Baker, D. J., Bolin, B., Dickinson, R. E., Goody, R. M., et al. (1979). *Carbon dioxide and climate: A scientific assessment*, pp. 33. Washington, D.C: National Academy of Science.

Colman, R., & McAvaney, B. (2009). Climate feedbacks under a very broad range of forcing. *Geophysical Research Letters*, *36*, L01702. https://doi.org/10.1029/2008GL036268

Cox, P. M., Huntingford, C., & Williamson, M. S. (2018). Emergent constraint on equilibrium climate sensitivity from global temperature variability. *Nature*, *553*, 319–322. https://doi.org/10.1038/nature25450

de Boer, B., Lourens, L. J., & van de Wal, R. S. (2014). Persistent 400,000-year variability of Antarctic ice volume and the carbon cycle is revealed throughout the Plio-Pleistocene. *Nature Communications*, *5*, 2999. https://doi.org/10.1038/ncomms3999

Etminan, M., Myhre, G., Highwood, E. J., & Shine, K. P. (2016). Radiative forcing of carbon dioxide, methane, and nitrous oxide: A significant revision of the methane radiative forcing. *Geophysical Research Letters*, *43*, 12,614–12,623. https://doi.org/10.1002/2016GL071930

Forster, P. M., Richardson, T., Maycock, A. C., Smith, C. J., Samset, B. H., Myhre, G., et al. (2016). Recommendations for diagnosing effective radiative forcing from climate models for CMIP6. *Journal of Geophysical Research: Atmospheres*, *121*, 12,460–12,475. https://doi.org/10.1002/2016JD025320

Friedrich, T., Timmermann, A., Tigchelaar, M., Elison Timm, O., & Ganopolski, A. (2016). Nonlinear climate sensitivity and its implications for future greenhouse warming. *Science Advances*, *2*(11), e1501923. https://doi.org/10.1126/sciadv.1501923

Ganopolski, A., & Brovkin, V. (2017). Simulation of climate, ice sheets and CO_2 evolution during the last four glacial cycles with an Earth system model of intermediate complexity. *Climate of the Past*, *13*(12), 1695–1716. https://doi.org/10.5194/cp-13-1695-2017

Ganopolski, A., & Calov, R. (2011). The role of orbital forcing, carbon dioxide and regolith in 100 kyr glacial cycles. *Climate of the Past*, *7*(4), 1415–1425. https://doi.org/10.5194/cp-7-1415-2011

Goodwin, P., Katavouta, A., Roussenov, V. M., Foster, G. L., Rohling, E. J., & Williams, R. G. (2018). Pathways to 1.5 °C and 2 °C warming based on observational and geological constraints. *Nature Geoscience*, *11*(2), 102–107. https://doi.org/10.1038/s41561-017-0054-8

Hasenclever, J., Knorr, G., Rüpke, L., Köhler, P., Morgan, J., Garofalo, K., et al. (2017). Sea level fall during glaciation stabilized atmospheric CO_2 by enhanced volcanic degassing. *Nature Communications*, *8*, 15867. https://doi.org/10.1038/ncomms15867

He, F. (2011). Simulating transient climate evolution of the last deglaciation with CCSM3 (PhD thesis). Madison: University of Wisconsin.

Huybers, P., & Langmuir, C. (2009). Feedback between deglaciation and volcanism, and atmospheric CO_2. *Earth and Planetary Science Letters*, *286*, 479–491. https://doi.org/10.1016/j.epsl.2009.07.014

Jouzel, J., Masson-Delmotte, V., Cattani, O., Dreyfus, G., Falourd, S., Hoffmann, G., et al. (2007). Orbital and millennial Antarctic climate variability over the last 800 000 years. *Science*, *317*, 793–796. https://doi.org/10.1126/science.1141038

Knutti, R., Rugenstein, M. A. A., & Hegerl, G. C. (2017). Beyond equilibrium climate sensitivity. *Nature Geoscience*, *10*(10), 727–736. https://doi.org/10.1038/ngeo3017

Köhler, P., Bintanja, R., Fischer, H., Joos, F., Knutti, R., Lohmann, G., & Masson-Delmotte, V. (2010). What caused Earth's temperature variations during the last 800,000 years? Data-based evidences on radiative forcing and constraints on climate sensitivity. *Quaternary Science Reviews*, *29*, 129–145. https://doi.org/10.1016/j.quascirev.2009.09.026

Köhler, P., de Boer, B., von der Heydt, A. S., Stap, L. S., & van de Wal, R. S. W. (2015). On the state dependency of equilibrium climate sensitivity during the last 5 million years. *Climate of the Past*, *11*, 1801–1823. https://doi.org/10.5194/cp-11-1801-2015

Köhler, P., Nehrbass-Ahles, C., Schmitt, J., Stocker, T. F., & Fischer, H. (2017). A 156 kyr smoothed history of the atmospheric greenhouse gases CO_2, CH_4, and N_2O and their radiative forcing. *Earth System Science Data*, *9*, 363–387. https://doi.org/10.5194/essd-9-363-2017

Köhler, P., Stap, L. S., von der Heydt, A. S., de Boer, B., van de Wal, R. S. W., & Bloch-Johnson, J. (2017). A state-dependent quantification of climate sensitivity based on paleo data of the last 2.1 million years. *Paleoceanography*, *32*, 1102–1114. https://doi.org/10.1002/2017PA003190

Kutzbach, J. E., He, F., Vavrus, S. J., & Ruddiman, W. F. (2013). The dependence of equilibrium climate sensitivity on climate state: Applications to studies of climates colder than present. *Geophysical Research Letters*, *40*, 3721–3726. https://doi.org/10.1002/grl.50724

Laskar, J., Robutel, P., Joutel, F., Gastineau, M., Correia, A. C. M., & Levrard, B. (2004). A long term numerical solution for the insolation quantities of the Earth. *Astronomy and Astrophysics*, *428*, 261–285. https://doi.org/10.1051/0004-6361:20041335

Lisiecki, L. E., & Raymo, M. E. (2005). A Pliocene-Pleistocene stack of 57 globally distributed benthic $\delta^{18}O$ records. *Paleoceanography*, *20*, PA1003. https://doi.org/10.1029/2004PA001071

Liu, Z., Otto-Bliesner, B. L., He, F., Brady, E. C., Tomas, R., Clark, P. U., et al. (2009). Transient simulation of last deglaciation with a new mechanism for Bølling-Allerød warming. *Science*, *325*(5938), 310–314. https://doi.org/10.1126/science.1171041

Lund, D. C., & Asimow, P. D. (2011). Does sea level influence mid-ocean ridge magmatism on Milankovitch timescales? *Geochemistry, Geophysics, Geosystems*, *12*, Q12009. https://doi.org/10.1029/2011GC003693

Myhre, G., Highwood, E. J., Shine, K. P., & Stordal, F. (1998). New estimates of radiative forcing due to well mixed greenhouse gases. *Geophysical Research Letters*, *25*(14), 2715–2718. https://doi.org/10.1029/98GL01908

PALAEOSENS-Project Members (2012). Making sense of palaeoclimate sensitivity. *Nature*, *491*, 683–691. https://doi.org/10.1038/nature11574

Past Interglacials Working Group of PAGES (2016). Interglacials of the last 800,000 years. *Reviews of Geophysics*, *54*(1), 162–219. https://doi.org/10.1002/2015RG000482

Peltier, W. R. (2004). Global glacial isostasy and the surface of the ice-age Earth: The ICE-5G (VM2) model and GRACE. *Annual Review in Earth and Planetary Sciences*, *32*, 111–149. https://doi.org/10.1146/annurev.earth.32.082503.144359

Pfister, P. L., & Stocker, T. F. (2017). State-dependence of the climate sensitivity in Earth system models of intermediate complexity. *Geophysical Research Letters*, *44*, 10,643–10,653. https://doi.org/10.1002/2017GL075457

Rohling, E. J., Marino, G., Foster, G. L., Goodwin, P., von der Heydt, A., & Köhler, P. (2018). Comparing climate sensitivity, past and present. *Annual Review of Marine Science*, *10*, 261–288. https://doi.org/10.1146/annurev-marine-121916-063242

Snyder, C. W. (2016). Evolution of global temperature over the past two million years. *Nature*, *538*(7624), 226–228. https://doi.org/10.1038/nature19798

Stap, L. B., van de Wal, R. S. W., de Boer, B., Köhler, P., Hoencamp, J. H., Lohmann, G., et al. (2018). The influence of land ice and CO_2 on polar amplification and specific equilibrium climate sensitivity during the past 5 million years. *Paleoceanography and Paleoclimatology*, *33*, 381–394. https://doi.org/10.1002/2017PA003313

Veres, D., Bazin, L., Landais, A., Toyé Mahamadou Kele, H., Lemieux-Dudon, B., Parrenin, F., et al. (2013). The Antarctic ice core chronology (AICC2012): An optimized multi-parameter and multi-site dating approach for the last 120 thousand years. *Climate of the Past*, *9*(4), 1733–1748. https://doi.org/10.5194/cp-9-1733-2013

von der Heydt, A. S., Dijkstra, H. A., van de Wal, R. S. W., Caballero, R., Crucifix, M., Foster, G. L., et al. (2016). Lessons on climate sensitivity from past climate changes. *Current Climate Change Reports*, *2*, 148–158. https://doi.org/10.1007/s40641-016-0049-3

Yoshimori, M., Hargreaves, J. C., Annan, J. D., Yokohata, T., & Abe-Ouchi, A. (2011). Dependency of feedbacks on forcing and climate state in physics parameter ensembles. *Journal of Climate*, *24*(24), 6440–6455. https://doi.org/10.1175/2011JCLI3954.1

Zeebe, R. E. (2013). Time-dependent climate sensitivity and the legacy of anthropogenic greenhouse gas emissions. *Proceedings of the National Academy of Sciences*, *110*(34), 13,739–13,744. https://doi.org/10.1073/pnas.1222843110

Supporting Information for "The effect of obliquity-driven changes on paleoclimate sensitivity during the late Pleistocene"

DOI: 10.1029/2018GL077717

Peter Köhler[1], Gregor Knorr[1], Lennert B. Stap[1], Andrey Ganopolski[2], Bas de Boer[3], Roderik S. W. van de Wal[3], Stephen Barker[4], Lars H. Rüpke[5]

[1]Alfred-Wegener-Institut Helmholtz-Zentrum für Polar-und Meeresforschung (AWI), P.O. Box 12 01 61, 27515 Bremerhaven, Germany
[2]Potsdam Institute for Climate Impact Research (PIK), Potsdam, Germany
[3]Institute for Marine and Atmospheric research Utrecht (IMAU), Center for Extreme Matter and Emergent Phenomena, Utrecht University, Princetonplein 5, 3584 CC Utrecht, The Netherlands
[4]School of Earth and Ocean Science, Cardiff University, UK
[5]GEOMAR Helmholtz Centre for Ocean Research Kiel, Wischhofstr. 1-3, 24159 Kiel, Germany

Contents of this file

References

de Boer, B., L. J. Lourens, and R. S. van de Wal (2014), Persistent 400,000-year variability of Antarctic ice volume and the carbon cycle is revealed throughout the Plio-Pleistocene, *Nature Communications*, *5*, 2999, doi:10.1038/ncomms3999.

Laskar, J., P. Robutel, F. Joutel, M. Gastineau, A. C. M. Correia, and B. Levrard (2004), A long term numerical solution for the insolation quantities of the Earth, *Astronomy and Astrophysics*, *428*, 261–285, doi:10.1051/0004-6361:20041335.

Corresponding author: Peter Köhler, `Peter.Koehler@awi.de`

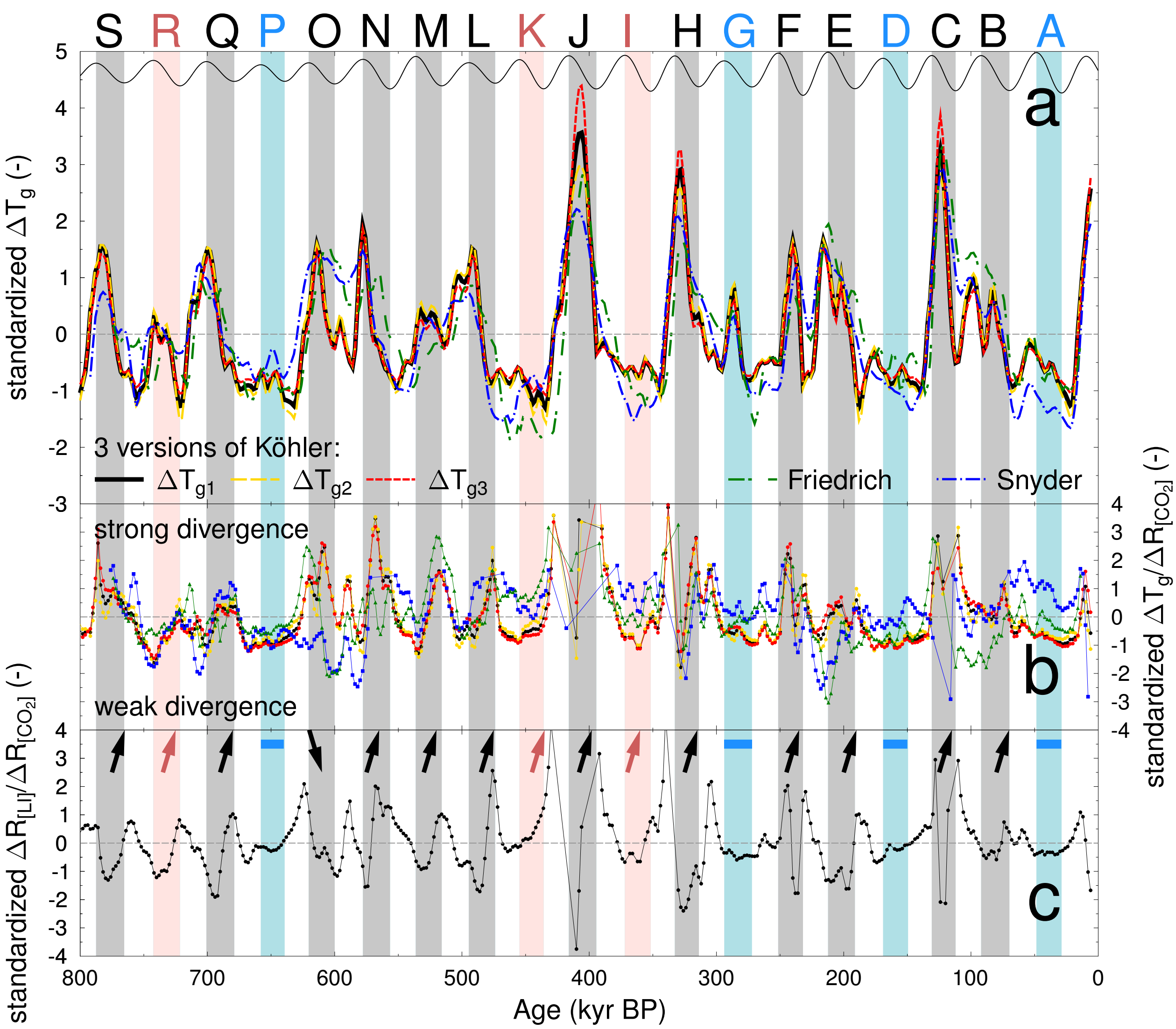

Figure S1. Same as Figure 3 (multi-millennial ΔT_g-CO_2 divergence, all data as 8-kyr running mean), but for different ΔT_g data sets: the 3 versions of ΔT_g obtained in Köhler (K2015), and proxy-based reconstruction of ΔT_g from Snyder and Friedrich (F2016). (a) ΔT_g; (b) divergence of ΔT_g and CO_2 indicated by the ratio $\Delta T_g/\Delta R_{[CO_2]}$. (c) relative land ice (sea level) contribution with respect to CO_2 ($\Delta R_{[LI]}/\Delta R_{[CO_2]}$). All data sets are identical in their ratio $\Delta R_{[LI]}/\Delta R_{[CO_2]}$, therefore only one respresentation is shown. All data sets have been standardized and outliers in the ratios in sub-figures (b, c) have been filtered out. Obliquity [*Laskar et al.*, 2004] is sketched on top of sub-panel a (thin black line), with shadings and labels (A–S) indicating times with decreasing obliquity. For more details see caption to Figure 3.

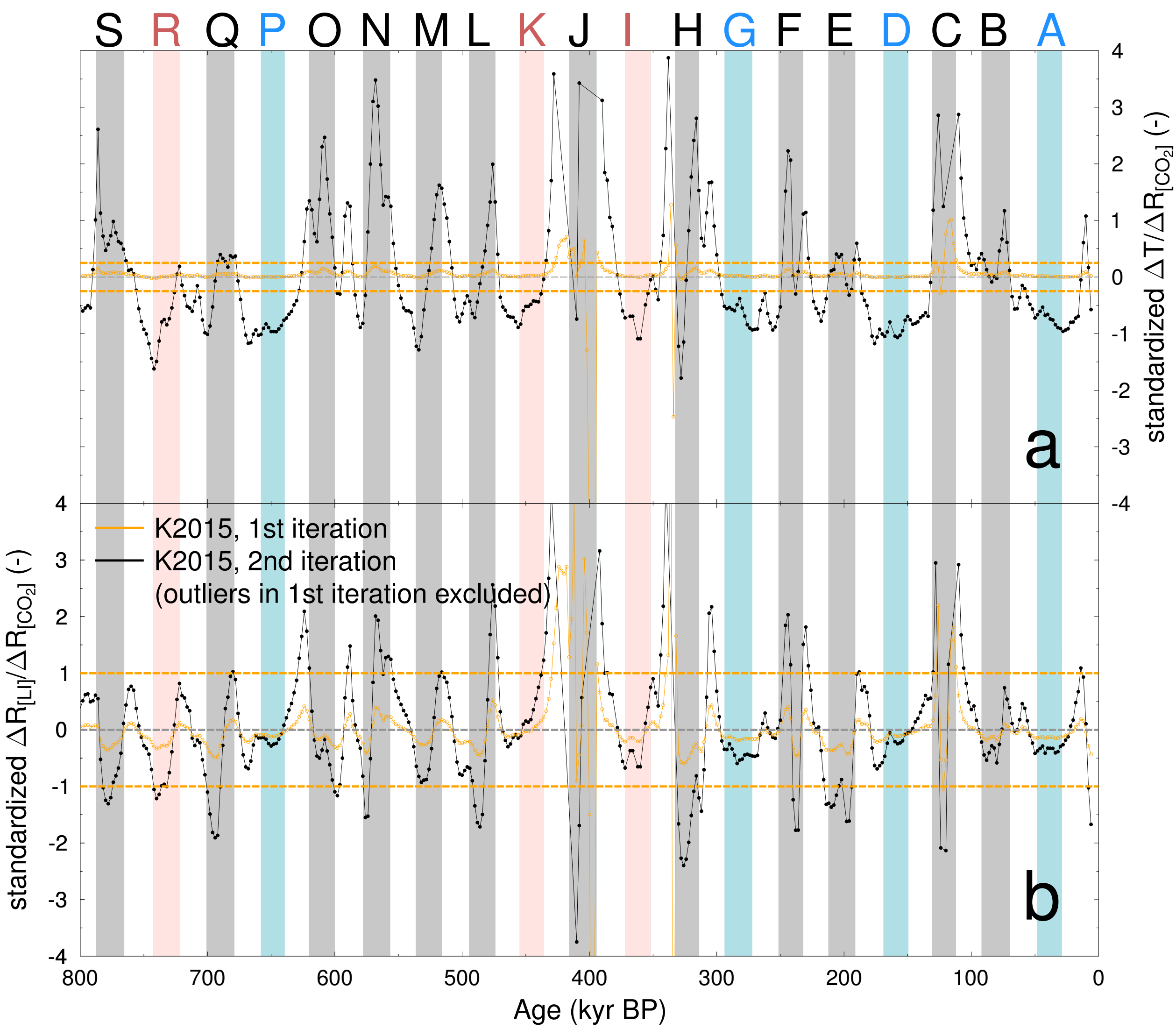

Figure S2. Illustration of outliers in standardizing procedures for K2015 and (a) ratio $\Delta T_g/\Delta R_{[CO_2]}$; (b) ratio $\Delta R_{[LI]}/\Delta R_{[CO_2]}$. The first iteration of standardization (orange lines) led to time series in these ratios which were dominated by a few data points from interglacials (e.g. -19 around 400 kyr BP in $\Delta T_g/\Delta R_{[CO_2]}$). Therefore the given threshold (horizontal orange lines) have been defined in order to leave these dominating individual ratios from interglacials in MIS 5. 9. 11 out of the further analysis, which is then based on a second standardization (black lines). Shadings and labels (A–S) indicating times with decreasing obliquity. For more details see caption to Figure 3.

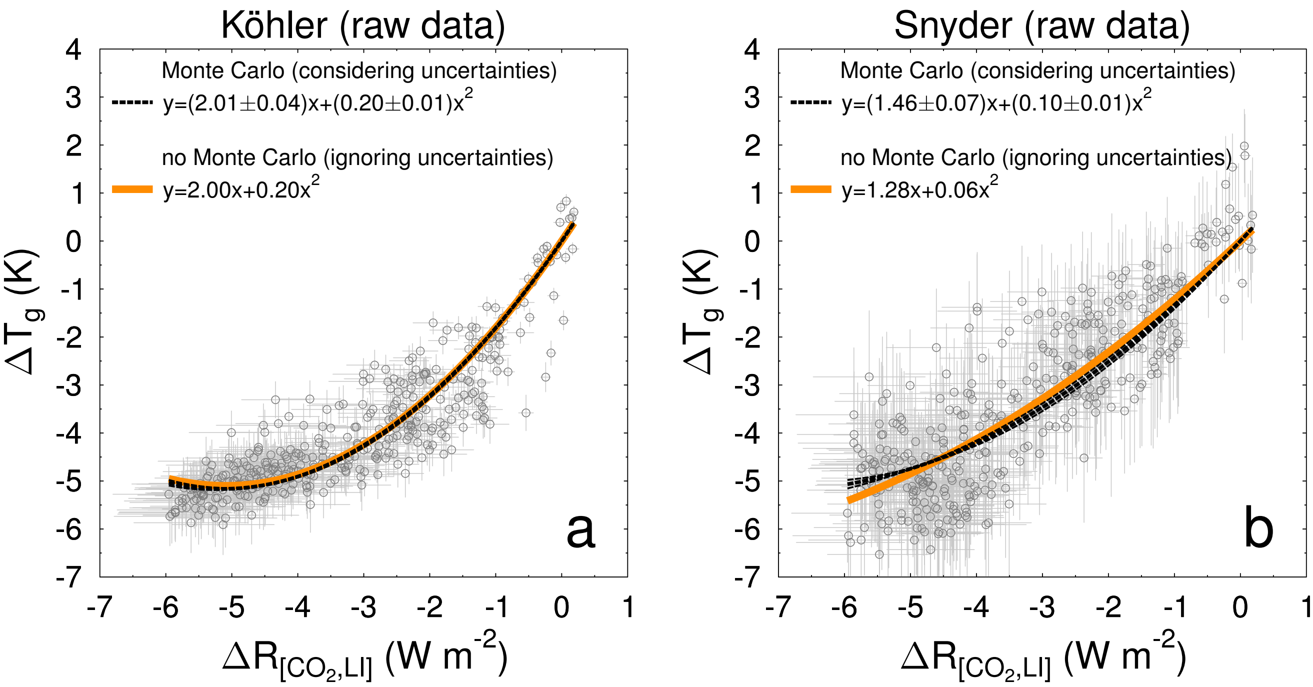

Figure S3. Comparing the influence of considering uncertainties in both x and y direction for non-linear fits by applying Monte Carlo (MC) statistics in scatter-plots of temperature change ΔT_{g} over radiative forcing change $\Delta R_{[\mathrm{CO_2,LI}]}$. Data are randomly resampled 5000 times in MC. The alternative fits without MC, which ignore uncertainties in both directions, are based only on the mean values. Applied on raw data from (a) Köhler (K2015), and (b) ΔT_{g} Snyder. Uncertainties show 1σ.

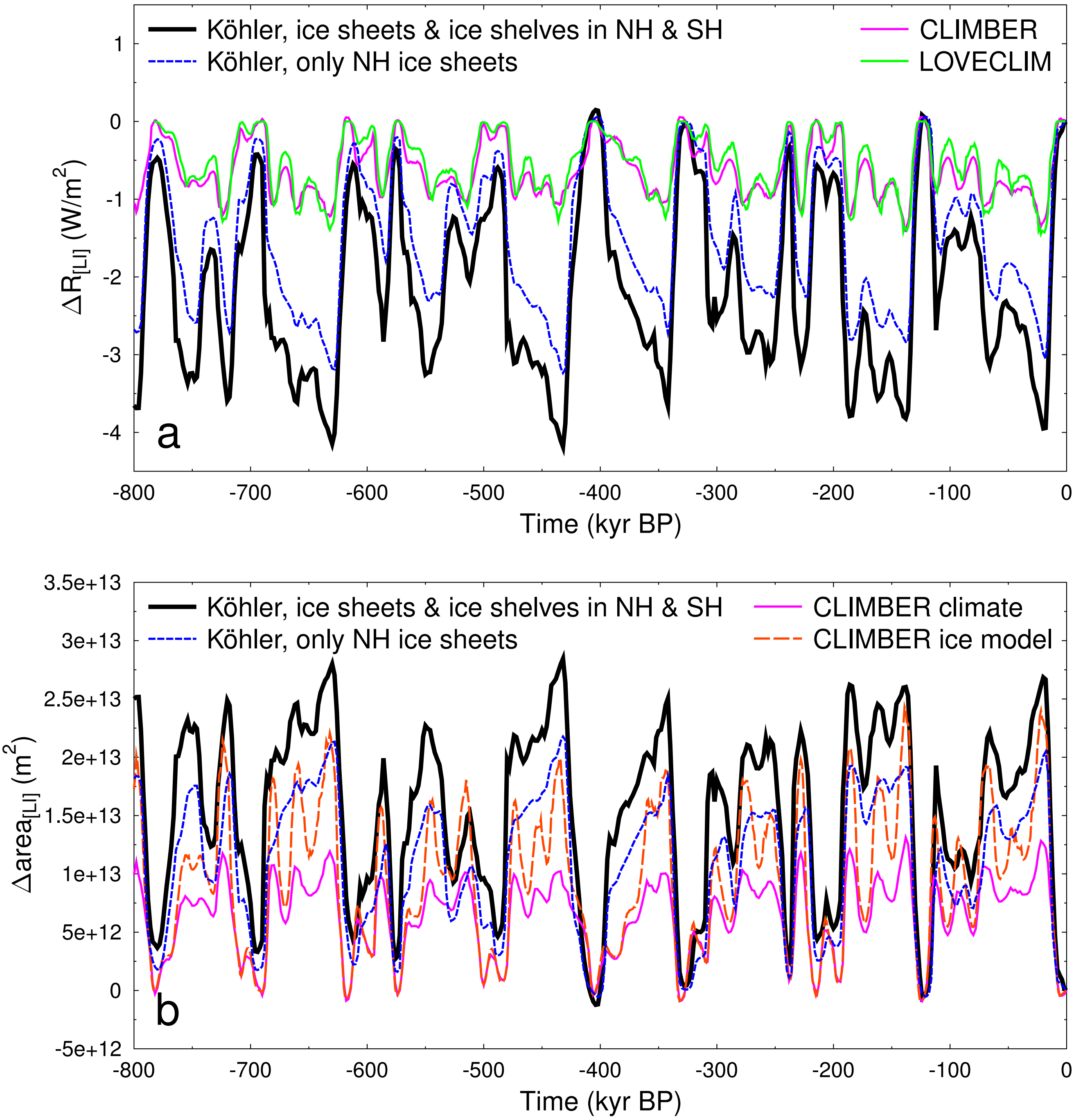

Figure S4. Differences in land ice sheets in various approaches. K2015 (Köhler) calculates changes of both ice sheets and ice shelves in northern (NH) and southern (SH) hemisphere, while both CLIMBER and LOVECLIM use the same ice sheet output generated within CLIMBER, which is restricted to NH ice sheets only. (a) $\Delta R_{[LI]}$ as published in K2015, and recalculated from *de Boer et al.* [2014] when restricted to NH ice sheets in comparison to $\Delta R_{[LI]}$ calculated internally in CLIMBER and LOVECLIM. (b) Change in underlying land ice area. In CLIMBER the land ice sub-module and the climate sub-module are fed with different land ice areas.

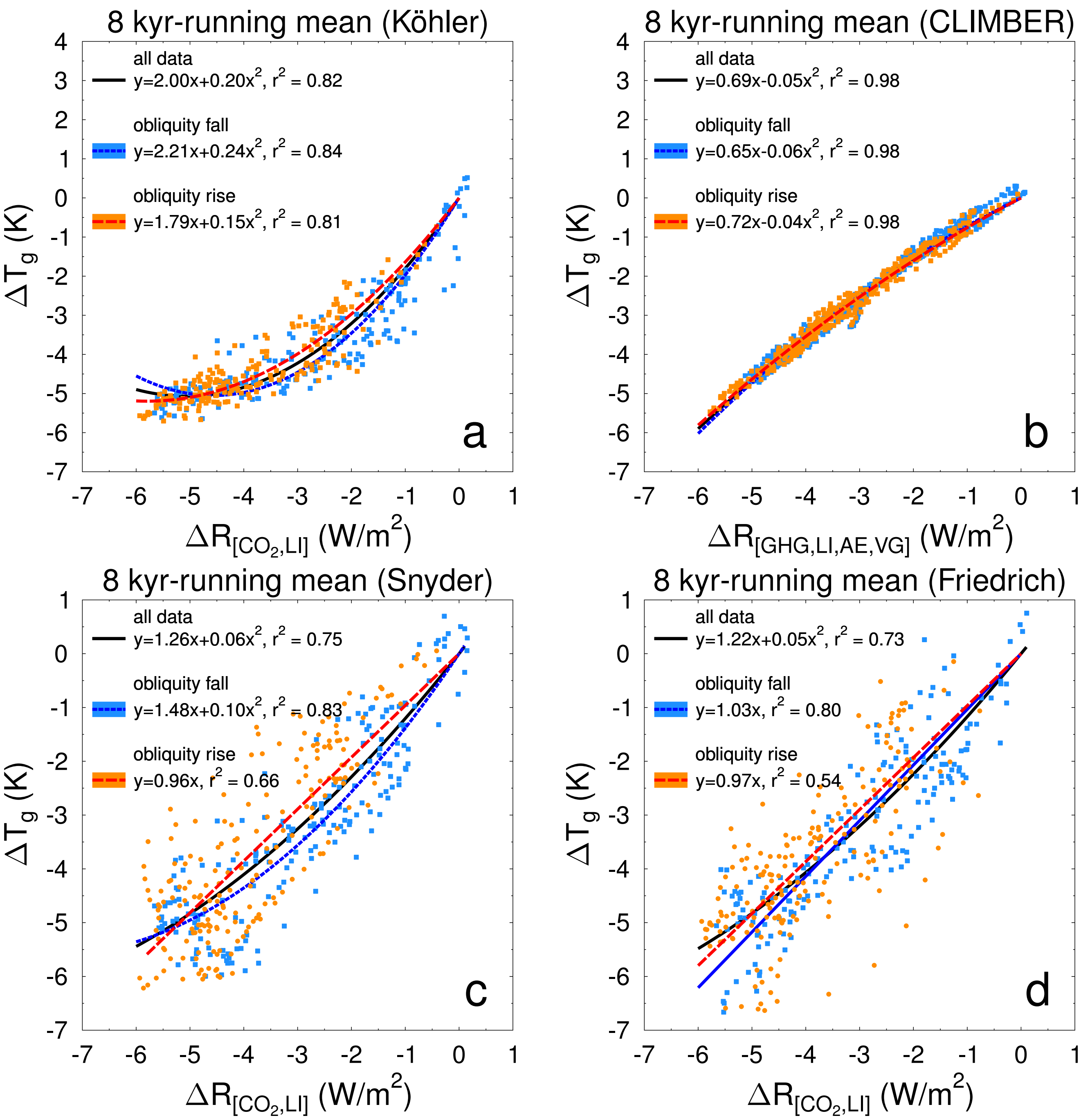

Figure S5. Scatter-plots of temperature change ΔT_g over radiative forcing change $\Delta R_{[X]}$. Multi-millennial (8-kyr running mean) effects split in time windows with falling or rising obliquity for (a) Köhler (K2015), (b) CLIMBER simulation results, (c) ΔT_g from Snyder and (d) ΔT_g from Friedrich (F2016). For CLIMBER the internally consistent results are shown, containing radiative forcing of all three greenhouse gases (GHG), and albedo changes based on land ice (LI), aerosols (AE) and vegetation (VG).

Table S1. Fitting a linear or a non-linear function to the data. For all data least-square linear ($y(x) = bx$) or non-linear regressions ($y(x) = bx + cx^2$) are calculated, and F-tests are used to determine the better fitting regression model. Additionally, for ΔT_g from K2015 and Snyder 5000 Monte-Carlo-generated (MC) realisations of the scattered $\Delta T_g - \Delta R_{[CO_2,LI]}$ were analysed. The data are randomly picked from the entire Gaussian distribution described by the 1σ of the given uncertainties in both ΔT_g and $\Delta R_{[CO_2,LI]}$. For MC the parameter values of fitted polynomials are given as mean±1σ uncertainty from the different realisations. n: number of data points in data set. χ^2: weighted sum of squares following either a linear fit (1st order) or a non-linear fit (2nd order polynomial). F: F-ratio for F-test to determine, if the higher order fit describes the data better than the lower order fit (1st versus 2nd order polynomial). p: p-value of the F-test. L: significance level of F-test: /: not significant ($p > 0.001$); *: significant at 0.1% level ($p \leq 0.001$). r^2: coefficient of determination of the fit. b,c: derived coefficients of fitted polynomial. 8-kyr rm: 8-kyr running mean.

Data set	n	χ^2		F	p	L	r^2	b	c	Figure
		1st	2nd				%			
no Monte-Carlo (neglecting uncertainties)										
K2015 ΔT_{g1}, all data, raw	394	376	148	603.9	<0.001	*	80	2.00	0.20	2b, S3a
K2015 ΔT_{g1}, all data, 8-kyr rm	389	333	112	764	<0.001	*	82	2.00	0.20	2f, S5a
K2015 ΔT_{g1}, strong divergence, 8-kyr rm	147	113	34	336.9	<0.001	*	81	2.28	0.26	2f
K2015 ΔT_{g1}, weak divergence, 8-kyr rm	217	63	27	286.7	<0.001	*	90	1.59	0.12	2f
K2015 ΔT_{g1}, obliquity fall, 8-kyr rm	188	211	61	457.4	<0.001	*	84	2.21	0.24	S5a
K2015 ΔT_{g1}, obliquity rise, 8-kyr rm	201	112	40	358.2	<0.001	*	81	1.79	0.15	S5a
Snyder ΔT_g, all data, raw[1]	400	357	333	28.7	<0.001	*	74	1.29	0.06	2b
Snyder ΔT_g, all data, raw[1]	394	352	329	27.4	<0.001	*	74	1.28	0.06	S3b
Snyder ΔT_g, all data, 8-kyr rm	396	324	304	25.9	<0.001	*	75	1.26	0.06	2g, S5c
Snyder ΔT_g, strong divergence, 8-kyr rm	169	87	75	26.7	<0.001	*	73	1.43	0.08	2g
Snyder ΔT_g, weak divergence, 8-kyr rm	147	60	60	0.0	0.878	/	80	0.82	0	2g
Snyder ΔT_g, obliquity fall, 8-kyr rm	196	136	110	45.9	<0.001	*	83	1.48	0.10	S5c
Snyder ΔT_g, obliquity rise, 8-kyr rm	200	176	175	0.8	0.389	/	66	0.96	0	S5c
Friedrich ΔT_g, all data, raw	385	378	356	23.7	<0.001	*	70	1.27	0.06	2b
Friedrich ΔT_g, all data, 8-kyr rm	381	319	304	18.9	<0.001	*	73	1.22	0.05	2h, S5d
Friedrich ΔT_g, strong divergence, 8-kyr rm	152	68	62	14.5	<0.001	*	80	1.37	0.06	2h
Friedrich ΔT_g, weak divergence, 8-kyr rm	198	82	82	0.1	0.798	/	80	0.88	0	2h
Friedrich ΔT_g, obliquity fall, 8-kyr rm	190	135	128	10.4	0.002	/	80	1.03	0	S5d
Friedrich ΔT_g, obliquity rise, 8-kyr rm	191	178	173	6.3	0.01	/	54	0.97	0	S5d
CLIMBER ΔT_g, all data, raw	400	176	170	14.5	<0.001	*	80	0.62	−0.03	2c
CLIMBER consistent, all data, raw	799	170	153	487	<0.001	*	94	0.75	−0.17	2e
CLIMBER consistent, all data, 8-kyr rm	792	44	24	658.3	<0.001	*	98	0.69	−0.05	S5b
CLIMBER consistent, obliquity fall, 8-kyr rm	388	25	12	418.2	<0.001	*	98	0.65	−0.06	S5b
CLIMBER consistent, obliquity rise, 8-kyr rm	404	19	11	292.4	<0.001	*	98	0.72	−0.04	S5b
LOVECLIM ΔT_g, all data, raw	389	200	199	1.9	0.164	/	85	1.04	0	2c
LOVECLIM consistent, all data, raw	739	126	126	0.01	0.939	/	94	1.96	0	2e
LOVECLIM/Friedrich ΔT_g, all data, raw	389	165	161	7.2	0.008	/	86	1.01	0	2d
CCSM (Trace21K) ΔT_g, all data, raw	209	21	10	227.7	<0.001	*	98	0.44	−0.07	2d
with Monte-Carlo (including uncertainties)										
K2015 ΔT_{g1}, all data, raw	394	3027	1334	497.5	<0.001	*	68	2.01±0.03	0.20±0.01	S3a
Snyder ΔT_g, all data, raw	394	729	659	41.6	<0.001	*	49	1.46±0.07	0.10±0.01	S3b

1: Both analyses differ slightly by the underlying data. In Fig. S5 the data set is reduced to those time steps also used in K2015 (for a few time periods no CO_2 data exist), otherwise no $\sigma_{\Delta R}$ is available, while in Fig. 2b the missing CO_2 have been generated by interpolation.